COMPASsCO$_2$

COMPONENTS' AND MATERIALS' PERFORMANCE FOR ADVANCED SOLAR SUPERCRITICAL CO2 POWERPLANTS

Demonstration of new Cr silicides and production as coupons for WP4 testing

Deliverable Number: 3.2

WP3: Materials Development

Date: November 4th, 2022

Deliverable type: Report

Dissemination level: Public

Lead participant: DECHEMA Forschungsinstitut (DFI)

This project has received funding from the European Union's Horizon 2020 Research and Innovation Action (RIA) under grant agreement No. **958418.**

AUTHORS

Name	Organization
Michael Kerbstadt, Ceyhun Oskay, Emma White, Mathias Galetz	Dechema (DFI)
Tom Blackburn, Kan Ma, Sandy Knowles	University of Birmingham (UoB)
Tatu Pinomaa	VTT

DOCUMENT HISTORY

Version	Date	Change
01	Nov. 04, 2022	Initial version uploaded

ABOUT THE PROJECT

COMPASsCO$_2$ is a 4-year HORIZON2020 project started on 1.11.2020. It is led by the German Aerospace Center (DLR), with eleven additional partners from seven European countries.

COMPASsCO$_2$ aims to integrate CSP particle systems into highly efficient s-CO$_2$ Brayton power cycles for electricity production. In COMPASsCO2, the key component for such an integration, i.e. the particle/s-CO$_2$ heat exchanger, will be validated in a relevant environment. To reach this goal, the consortium will produce tailored particle and alloy combinations that meet the extreme operating conditions in terms of temperature, pressure, abrasion and hot oxidation/carburization of the heat exchanger tubes and the particles moving around/across them. The proposed innovative CSP s-CO$_2$ Brayton cycle plants will be flexible, highly efficient, economic and 100% carbon neutral large-scale electricity producers.

The research focus of COMPASsCO2 is on three main technological improvements: development of new particles, development of new metal alloys and development of the heat exchanger section.

DISCLAIMER

This project has received funding from the European Union's Horizon 2020 Research and Innovation Action (RIA) under grant agreement No. **958418.**

TABLE OF CONTENTS

LIST OF FIGURES

LIST OF TABLES

LIST OF ABBREVIATIONS

COMPASsCO2	Components' and Materials' Performance for Advanced Solar Supercritical CO2 Power Plants
CST/CSP	Concentrating Solar Thermal/Concentrated Solar Power
EC	European Commission
EU	European Union
Cr	Chromium
Si	Silicon
Fe	Iron
Ni	Nickel
SEM	Scanning electron microscopy
EPMA	Electron probe microanalysis
XRD	X-ray diffraction

1 ABSTRACT

Cr-Si-alloys with a two-phase microstructure consisting of a toughening bcc-Cr_{ss}-matrix and strengthening, hard A15-Cr_3Si precipitates are promising materials for use in oxidative high temperature environments. Additionally, the formation of the hard intermetallic A15 Cr_3Si phase increases the hardness and the wear properties of the material. This suggests also good resistance against erosion under high temperatures, which makes Cr-Si-alloys interesting for the targeted heat exchanger environment. However, Cr-Si alloys have some drawbacks, which are currently excluding them from any structural applications. These are mainly the brittleness at lower temperatures due to the high ductile-to-brittle transition temperature (DBTT) and the evaporation of oxygen compounds and further embrittlement because of nitridation at temperatures >1000°C. To counteract these challenges and use such alloys as bulk materials it is necessary to find suitable alloying elements.

Within the task 3.2 the effect of Fe and Ni as ternary alloying elements to the Cr-Si-system was investigated. The two elements were systematically alloyed to the Cr_x Si_8-system. Especially the influence on the microstructure and mechanical properties was analysed. The alloys were produced by arc melting and afterwards subjected to a heat treatment at 1200°C for 100h to anneal the microstructure. During the heat treatment the Cr_3Si-phase precipitates from the supersaturated state. This effect increases the mechanical properties and hardness by precipitation hardening. In the focus of the conducted investigations is the microstructure evolution and the influence of Fe and Ni. This includes phase analysis by SEM, EPMA and XRD, nanoindentation as well as microhardness measurements. To investigate the influence of Fe and Ni to the DBTT and mechanical properties, compression tests at different temperatures were carried out. In parallel these alloy compositions lead to develop a system to be applied as coatings and to be used for the production of coated coupons for WP4, in accordance with the requirements (geometries and quantities) of each testing partner. These samples have been initiated and upon final completion, an updated report will be published.

2 RESULTS AND DISCUSSION

The target of task 3.2 is to develop materials that are suitable for use as tubes in the heat exchanger environment of the CSP. Therefore new Cr-Si alloys with additional alloying elements are investigated. The desired microstructure of the alloys consists of a toughening bcc Cr_{ss} matrix and hard intermetallic A15 Cr_3Si precipitates for increasing the mechanical properties and hardness of the alloys.

Various samples with different compositions were produced by arc melting, which are shown in Table 1. To be able to determine the influence of alloying by Fe and Ni, the Si amount was held constant at 8 at.%, while Cr and the alloying element were varied systematically. Former studies showed that by limiting the Si amount to 8 at.% coarse primary precipitates can be avoided. These precipitates would be disadvantageous for the mechanical properties (especially deformability). Due to this the alloys in the as-cast condition consist primarily and preferentially of an oversaturated single phase Cr_{ss}.

Table 1. Compositions of produced alloys (at.%).

Cr-Si-Fe	90-8-2	88-8-4	86-8-6	84-8-8	76-8-8	60-8-32
Cr-Si-Ni	90-8-2	88-8-4	86-8-6	84-8-8	76-8-8	60-8-32

To anneal the microstructure the alloys were subjected to a heat treatment at 1200° C for 100 h. During the heat treatment the intermetallic phase precipitates from the oversaturated Cr_{SS} via a diffusion controlled process. To maintain the microstructure formed at 1200°C, the samples were quenched by water directly after taking them out of the furnace.

Both the as-cast and heat treated alloys were analysed and characterized. Phase fractions were calculated on the base of element distribution images by EPMA. Phase compositions and properties were determined by EPMA spot measurements, SEM BSE images, and XRD measurements. Due to the constant erosion forces on the materials of the heat exchanger tubes the hardness properties of the investigated materials are essential. Hardness properties of the different phases were investigated by nanoindentation and the microhardness of the overall alloys by Vickers hardness measurements. The influence on the DBTT was determined by compression tests at different temperatures up to 800°C in air.

An overview of the currently achieved results is given in the following sections.

2.1 Cr-Si-Fe

2.1.1 Microstructure and phase analysis

In the as-cast condition, before conducting the heat treatment, all Cr-Si-Fe alloys showed a single phase Cr_{SS} microstructure (as confirmed by XRD). A representative cross section is shown in Figure 1.

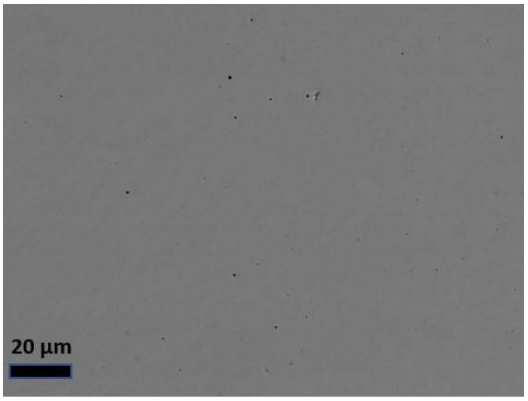

Figure 1. Representative optical microscopy cross-section image of an alloy in the as-cast condition, single phase Cr_{ss}.

Representative cross-sections of the alloys after heat treatment are shown in Figure 2. After the heat treatment the microstructure of all alloys up to Fe ≤ 16 at.% consists of Cr_{ss} and the

hardening Cr_3Si phase. The Cr_3Si phase precipitates along the grain boundaries as well as within the grains. Only the heat-treated $Cr_{60}Si_8Fe_{32}$ alloy still shows a single phase Cr_{ss} microstructure without any precipitates. The shape of the precipitates seems to change with further alloying of Fe. Determination of the phase compositions imply a change in the stoichiometry of the A15 phase for the different alloys, which could explain the difference in morphology.

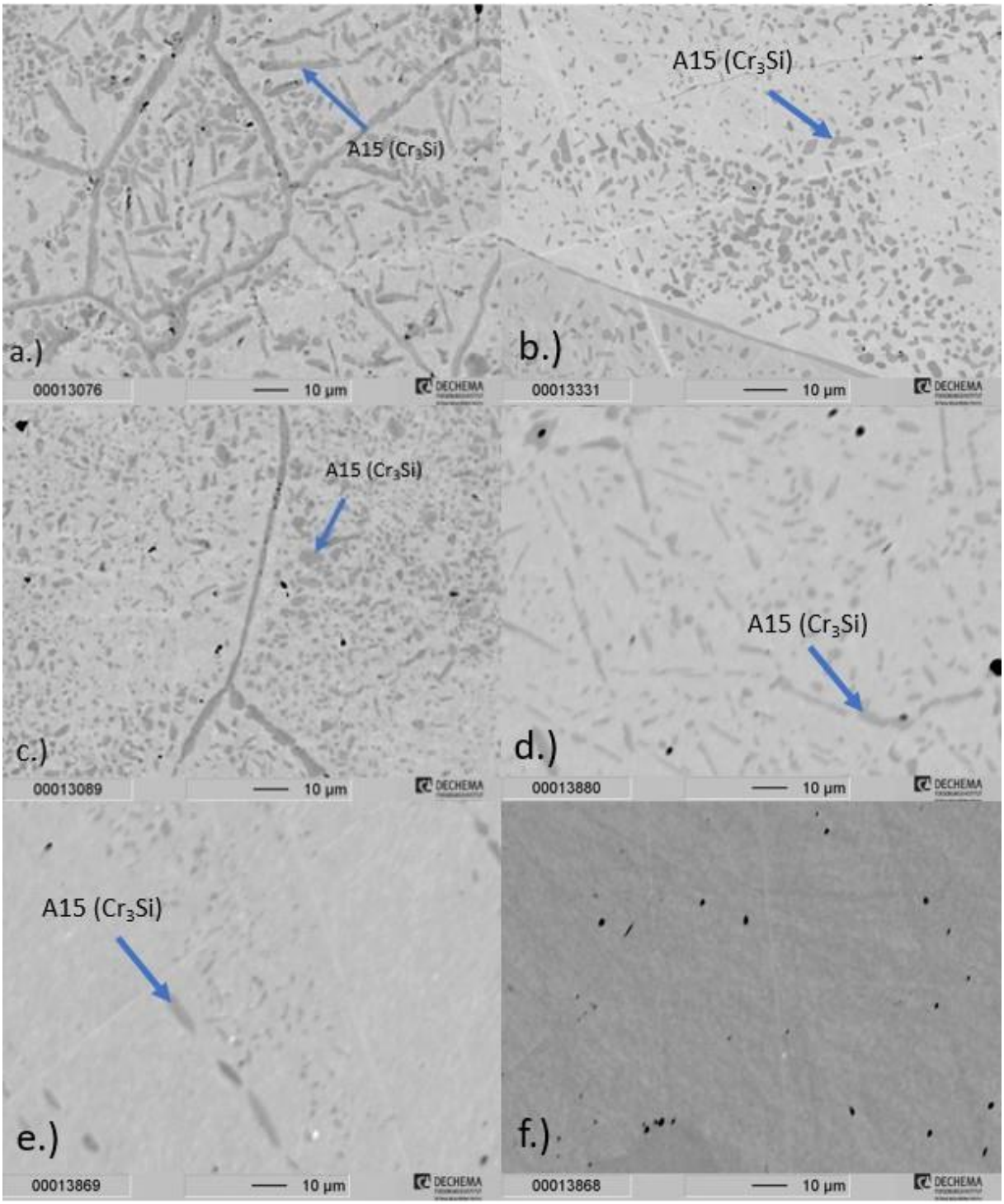

Figure 2. Representative cross sections of the heat-treated alloys: a.) $Cr_{90}Si_8Fe_2$, b.) $Cr_{88}Si_8Fe_4$, c.) $Cr_{86}Si_8Fe_6$, d.) $Cr_{84}Si_8Fe_8$, e.) $Cr_{76}Si_8Fe_{16}$, f.) $Cr_{60}Si_8Fe_{32}$.

The results of the quantitative phase fraction analysis are shown in Figure 3. With further

alloying of Fe the fraction of the A15 phase in the alloy decreases, which seems to follow an almost linear trend. From this observation it can be concluded that Fe stabilizes the Cr_{ss} phase. Also phase analysis conducted by EPMA spot measurements shows that Fe has a higher solubility in the Cr_{ss} phase compared to the Cr_3Si phase. Additionally Fe increases the solubility of Si in Cr_{ss}, resulting in that in the Fe_{32} alloy all 8 at.% Si can be dissolved and no A15 precipitates are formed.

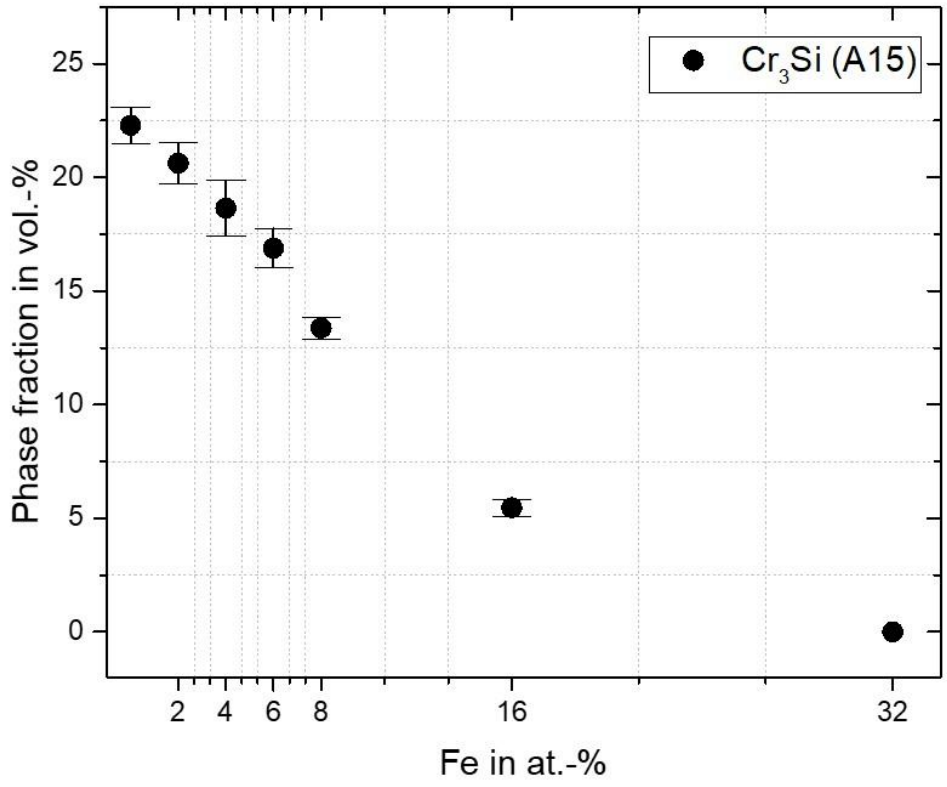

Figure 3. Phase fraction of the A15 Cr_3Si phase as a function of the Fe amount in the alloy.

2.1.2 Hardness measurements

Results of the Vickers microhardness measurements (HV 0.3) are shown in Figure 4. With alloying of Fe up to 16 at.% the microhardness increased by 35 % even though the fraction of the hardening A15 phase decreased. This can be attributed to solid solution hardening. With the higher amount of Fe in the alloy more Fe solid solution atoms are built into the bcc lattice of the Cr_{ss} which causes the hardening effect. In Figure 5 the nanohardness values of the different phases measured by nanoindentation are shown. The tendency of hardness to increase with Fe content is clearly visible. For the alloy with 32 at.% Fe a clear drop in hardness can be observed. This softening can be attributed to the absence of any precipitates in the alloy.

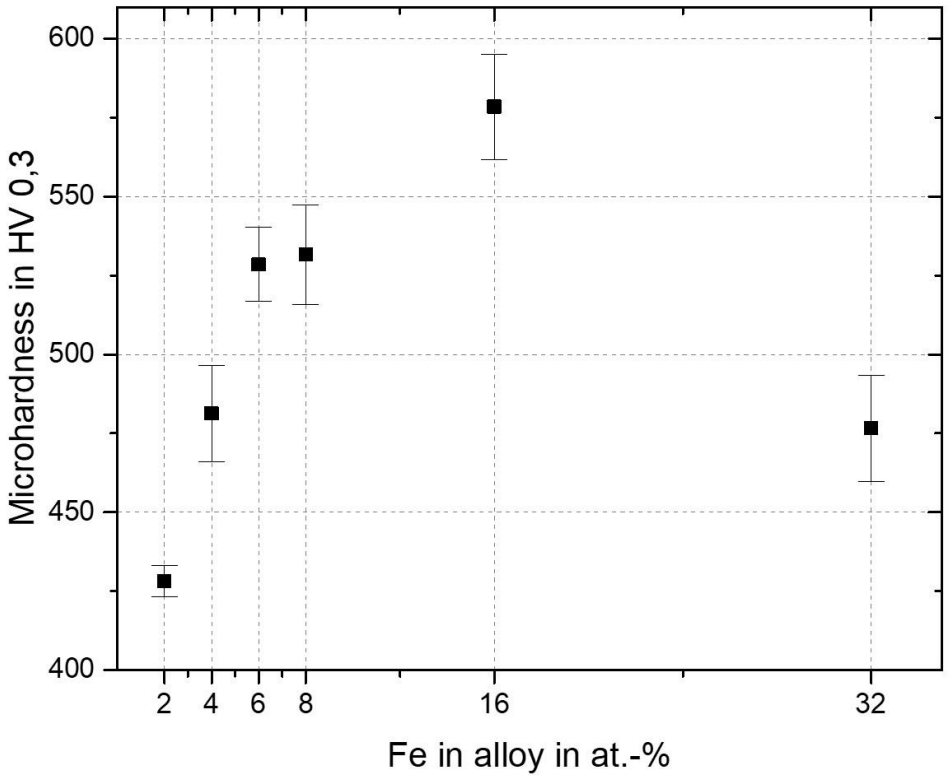

Figure 4. Phase fraction of the A15 Cr_3Si phase as a function of the Fe amount in the alloy.

In Figure 5 also a tendency for increasing hardness of the A15 phase can be seen. So the substitution of Cr by Fe seems to increase the hardness here as well. Phase analysis shows that the stoichiometry of the A15 phase changes, with most likely Fe substituting Cr in the lattice of the A15 phase

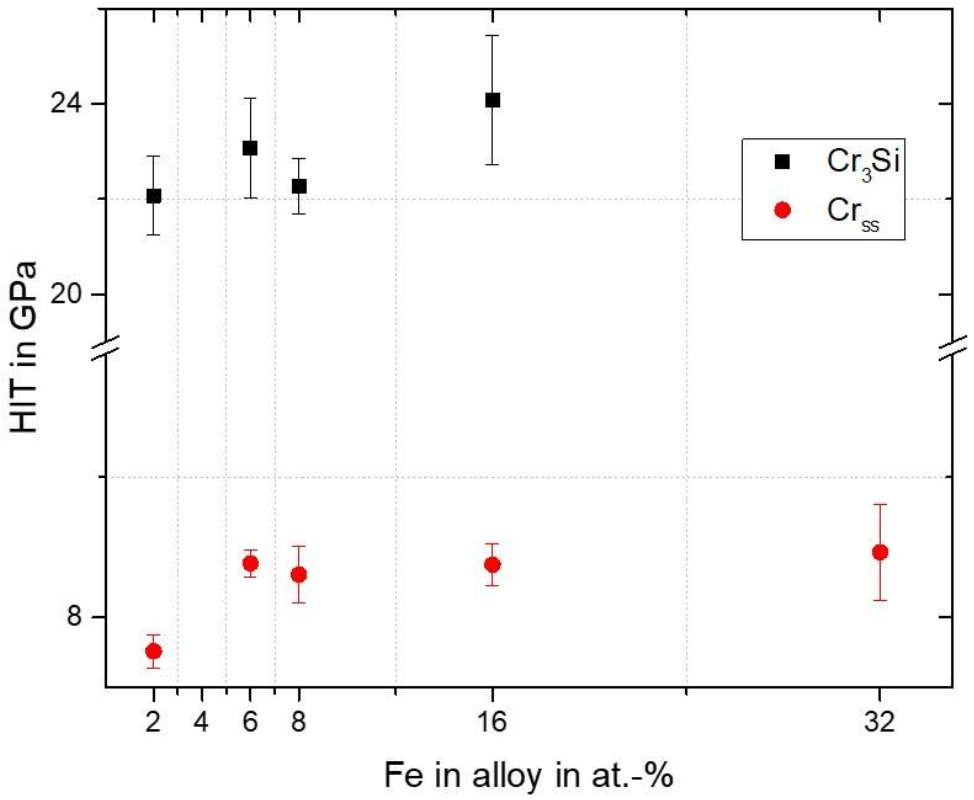

Figure 5. Nanoindentation measurements of the phases for the different alloys.

2.1.3 Mechanical testing: compression tests

To determine the influence of Fe alloying on the DBTT, compression tests at temperatures of 400°C, 500°C, 600°C and 700°C were performed. Due to the high effort to manufacture the specific cylindric samples, the tests were limited to the alloys with compositions of $Cr_{88}Si_8Fe_4$ and $Cr_{86}Si_8Fe_2$. As a reference, also samples of the composition $Cr_{92}Si_8$ were tested. In Figure 6 the compressive fracture percent deformation is plotted for the different temperatures. For each temperature a representative fractured sample is shown.

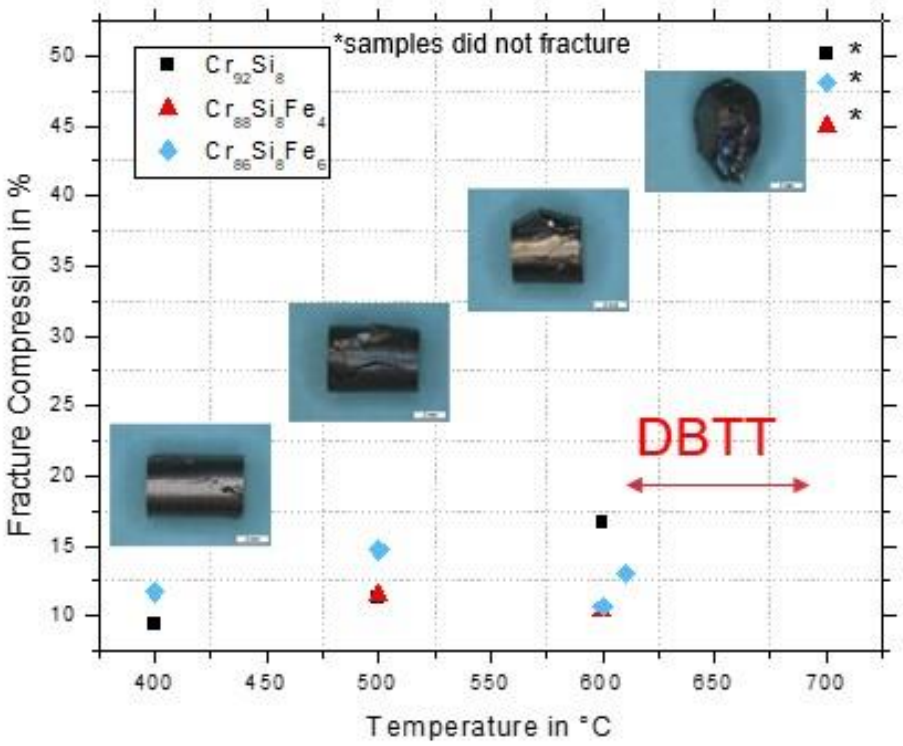

Figure 6. Results of compression tests conducted at different temperatures: Fracture compression and fracture patterns of the alloys in dependence of the testing temperatures.

It can be seen that for the samples fractured at 400°C, 500°C and 600°C no significant increase in deformation occurred and all samples showed a fracture pattern which can be considered as brittle. In contrast, samples of all alloy compositions at 700°C did not fracture at all and showed a very ductile behaviour. So it can be concluded that the DBTT for the tested alloys is somewhere in the temperature range between 600°C and 700°C. Accordingly, alloying with Fe does not seem to have a major influence on the DBTT.

2.2 Cr-Si-Ni

2.2.1 Microstructure and phase analysis

In the as-cast condition of the low alloyed materials (Ni = 2 at.%) a single phase Cr_{ss} microstructure is present. For alloys with Ni ≥ 6 at.% some primary precipitation of the σ ($Cr_{13}Ni_5Si_2$) phase can be detected along the grain boundaries. Representative cross-sections are shown in Figure 7.

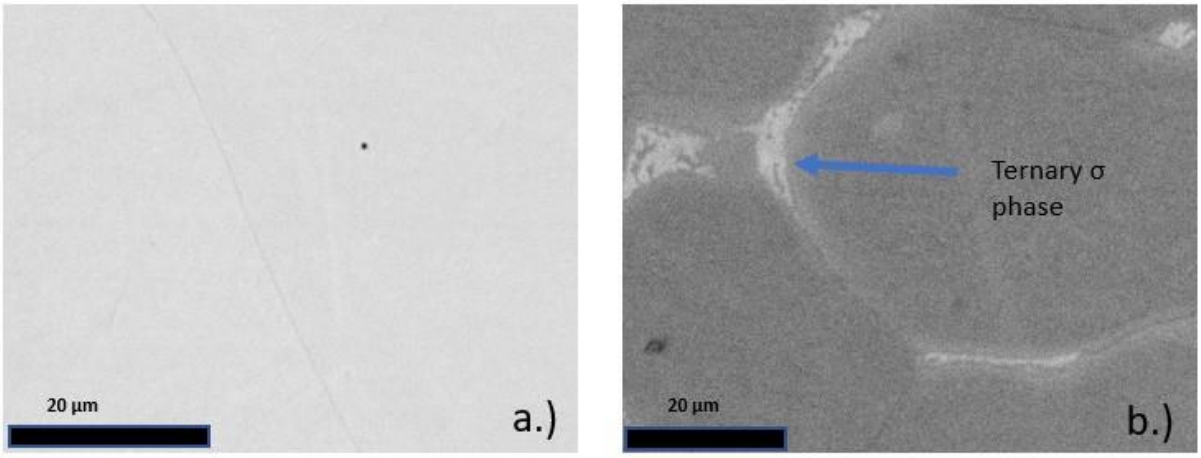

Figure 7. Cross-sections of alloys in the as-cast condition: a.) Single phase Cr_{ss} microstructure for alloys with Ni less than 4 at.%, b.) Cr_{ss} with σ grain boundary precipitates for alloys with Ni greater than 6 at.%.

Representative cross-sections for the different alloys after heat treatment are shown in Figure 8. Alloys with low amounts of Ni (<6 at.%) show the two phase microstructure consisting of bcc Cr_{ss} and intermetallic A15 Cr_3Si. With further alloying, the amount of the A15 precipitation phase decreases and also precipitates of the ternary σ phase, $Cr_{13}Ni_5Si_2$, can be observed. From literature, the $Cr_{13}Ni_5Si$ phase is recorded to have very good high temperature oxidation and wear behaviour, but conversely embrittles the materials when it is present in large quantities. Also a coarsening of the precipitates can be seen, which can be considered disadvantageous to the mechanical properties of the alloys. For the alloy with Ni = 16 at.% the microstructure changes into a two phase structure consisting of Cr_{ss} and σ $Cr_{13}Ni_5Si_2$. Further alloying up to 32 at.% Ni leads to a microstructure consisting of a $Cr_{13}Ni_5Si_2$ matrix and fcc Ni_{ss} precipitates.

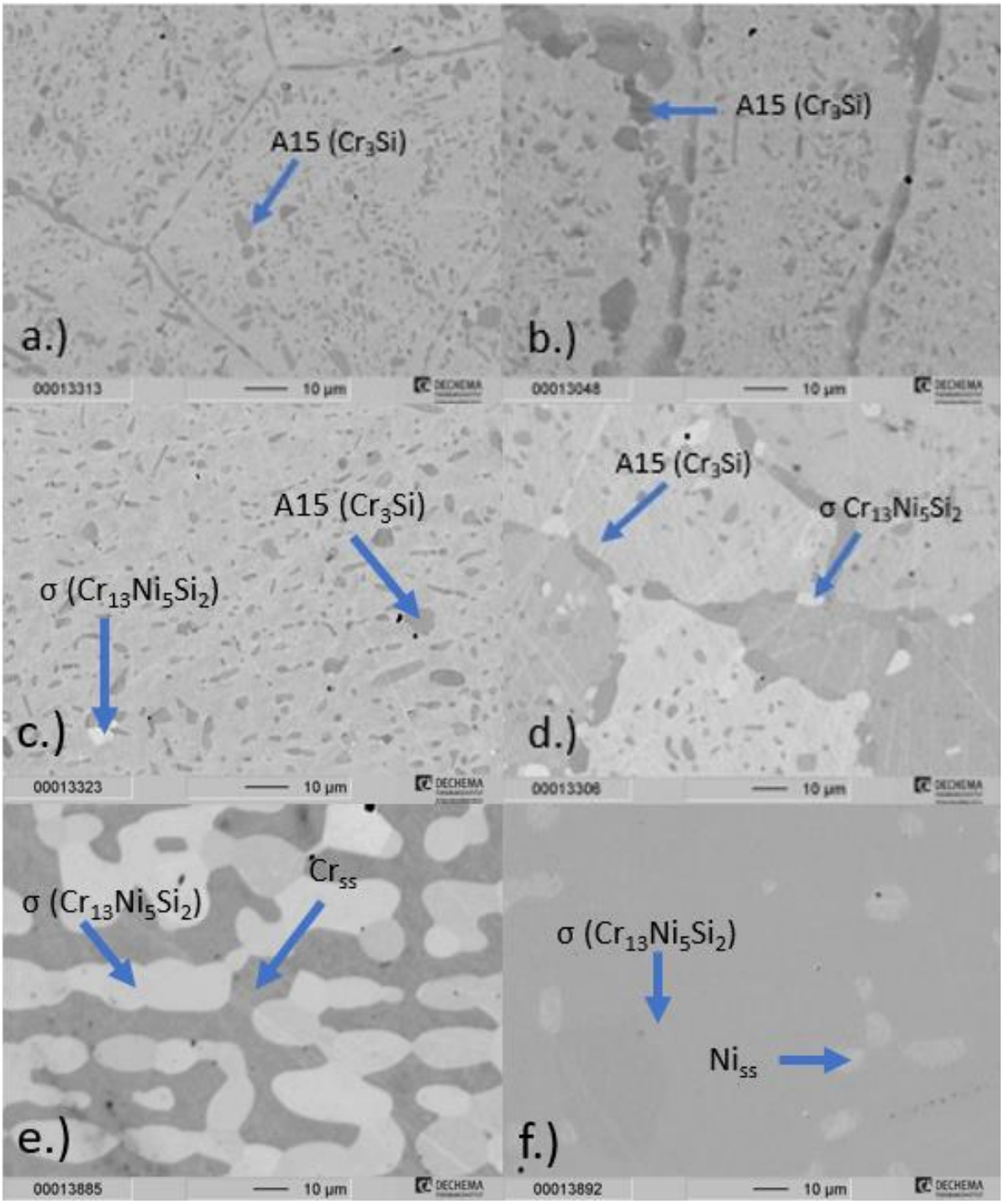

Figure 8. Representative cross-sections of heat-treated alloys: a.) $Cr_{90}Si_8Ni_2$, b.) $Cr_{88}Si_8Ni_4$, c.) $Cr_{86}Si_8Ni_6$, d.) $Cr_{84}Si_8Ni_8$, e.) $Cr_{76}Si_8Ni_{16}$, f.) $Cr_{60}Si_8Ni_{32}$.

The results of the quantitative phase fraction analysis are shown in Figure 9. With further alloying of Ni the fraction of A15 phase in the alloy decreases. From a content of 6 at.%, Ni can no longer be completely dissolved in Cr_{ss} and Cr_3Si, so the ternary σ phase also begins to precipitate. If the Ni content is then further increased, the fraction of the σ phase increases significantly, which is most likely to embrittle the alloys.

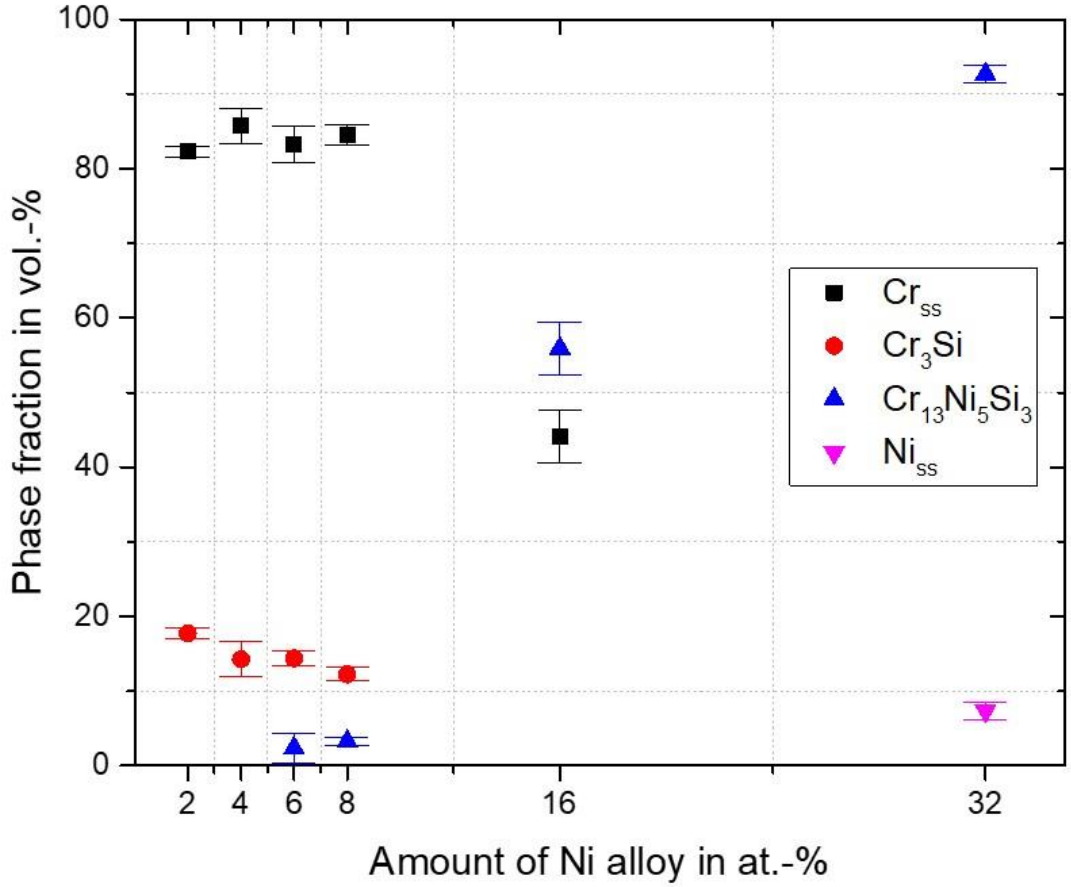

Figure 9. Phase fractions for the different alloy compositions as a function of Ni content.

2.2.2 Hardness measurements

The results of the Vickers microhardness measurements (HV 0.3) are shown in Figure 10. The hardness reaches a maximum for the alloy with 16 at.% Ni and is increased by 104% when compared to the $Cr_{90}Si_8Ni_2$ alloy. The hardness for the $Cr_{60}Si_8Ni_{32}$ then drops which is probably caused by the precipitation of the soft fcc Ni_{ss} phase. The higher increase in microhardness for the alloys with Ni when compared to the ones alloyed by Fe can be explained by the larger lattice misfit between Ni and Cr.

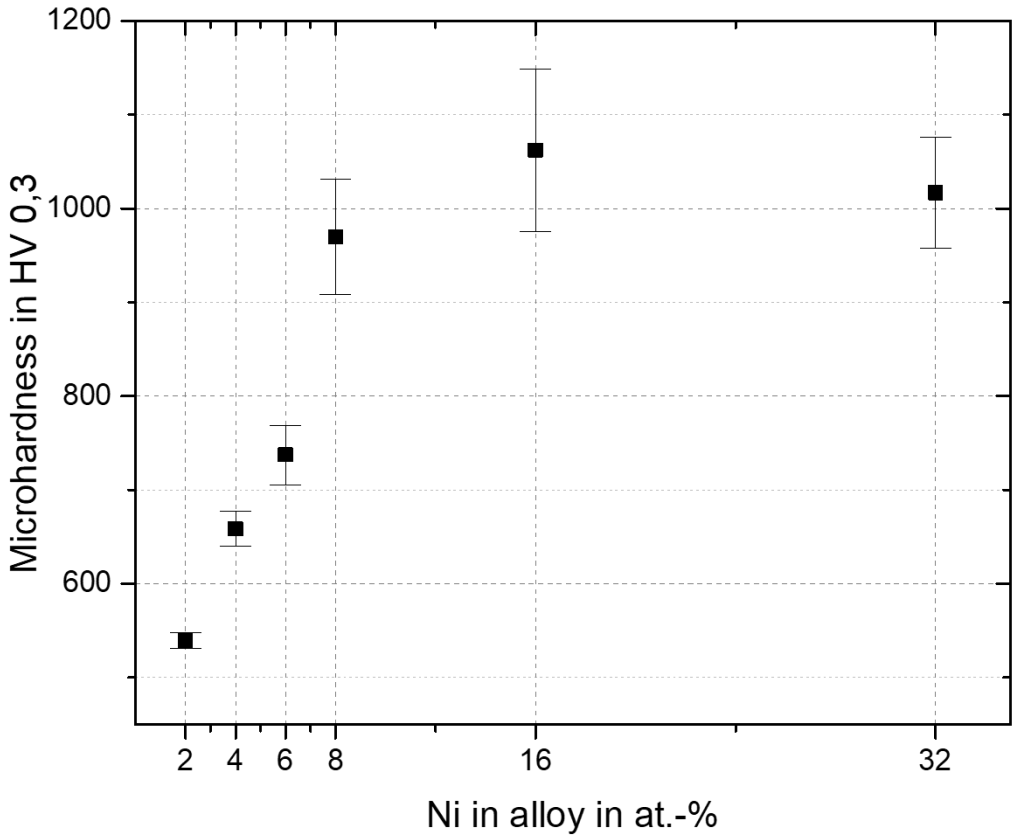

Figure 10. Microhardness of the different alloys as a function of Ni content.

The results of the nanohardness measurements are shown in Figure 11. For the Cr_{ss} phase a clear increase in hardness is visible which is caused by solid solution hardening. The hardness of the Cr_3Si and $Cr_{13}Ni_5Si_2$ phases decrease with higher amount of Ni in the alloy which can be attributed to changes in the stoichiometry of the phases. The Ni_{ss} is much softer compared to the other phases due to the fcc structure.

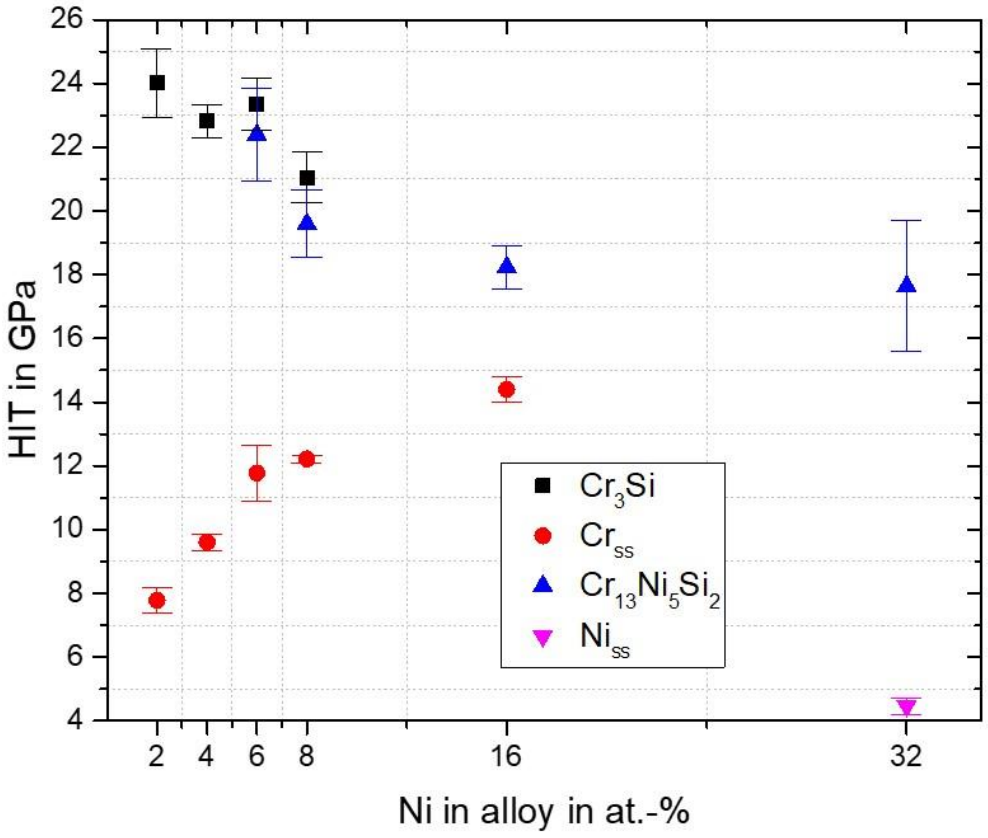

Figure 11. Nanoindentation measurements of the phases for the different alloys as a function of Ni content.

2.2.3 Mechanical testing: compression tests

To determine the DBTT of the alloys, compression tests of the alloys with the composition of $Cr_{88}Si_8Ni_4$ and $Cr_{86}Si_8Ni_6$ at 700°C and 800°C were conducted. The parameters of the tests were defined based on the previous results for the Cr-Si-Fe alloys (Section 2.1.3).

In Figure 12 the compression fracture percent deformation is plotted for the different temperatures. For each temperature and composition a representative fractured sample is shown.

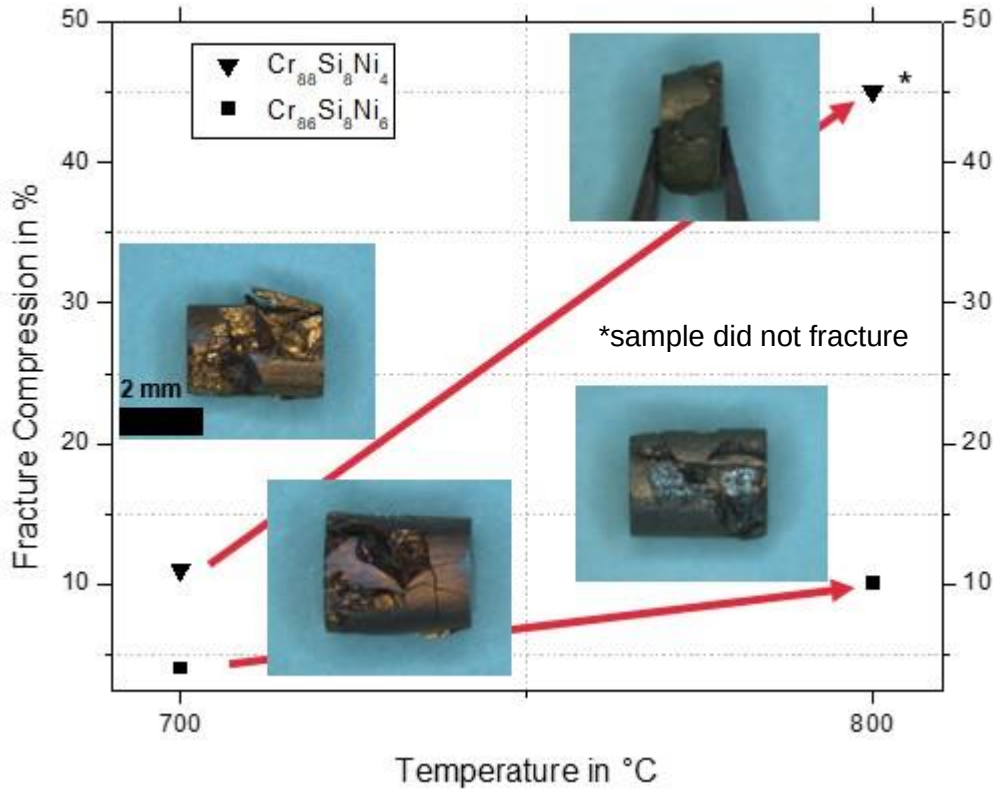

Figure 12. Results of compression tests conducted at different temperatures for the Cr-Si-Ni alloys: Fracture compression and fracture patterns of the alloys as a function of the testing temperatures.

Compared to the Cr-Si-Fe alloys, where all samples show very ductile behaviour at 700°C, the samples of the Cr-Si-Ni alloys still demonstrate brittle fracture at 700°C. At 800°C the $Cr_{88}Si_8Ni_4$ sample does not fracture and shows very high deformation. According to this, the DBTT can be estimated to be between 700°C and 800°C. However, the $Cr_{86}Si_8Ni_6$ sample fractures even at 800°C in a somewhat brittle manner and it is possible that the DBTT was not reached. So it can be concluded that alloying with higher amounts of Ni seems to embrittle the alloys and increases the DBTT.

3 CONCLUSIONS

Within the conducted investigations the influence of Fe and Ni as ternary alloying elements to the $Cr_xSi_8X_x$ could be shown. Both elements decrease the fraction of the hard intermetallic Cr_3Si phase. Alloying by Fe ≥ 32at.% leads to a single phase Cr_{SS} microstructure; alloying by Ni ≥ 6at.% leads to the additional precipitation of the intermetallic σ phase, $Cr_{12}Ni_5Si_2$. In small quantities this phase can increase the hardness and oxidation resistance of the alloys, but it can also lead to embrittlement.

The hardness of the materials could be increased significantly by alloying with both elements which can be considered as promising for the required erosion resistance within the targeted heat exchanger environment. The composition with the highest hardness was $Cr_{76}Si_8Ni_{16}$ with 1080 HV 0.3.

The conducted compression tests showed that the DBTT for all tested Fe-modified alloys is over 600°C and for the Ni-containing alloys even above at least 700°C. These high DBTTs and the risk of brittle failure at temperatures below is an exclusion criterion for use as a structural material for the tested Cr-Si-alloys. However, the benefits of high hardness and oxidation resistance of this material system could still be optimally exploited within the heat exchanger tubes as Cr-Si diffusion coatings on Fe- or Ni-based state of the art materials (Task 3.3.). Therefore, the studies conducted here and the results obtained are still significant in terms of the overall development process. Under the organization of the project coordinator and the WP3 and WP4 leaders, Cr-Si diffusion coatings on state-of-the-art materials with the different required geometries for exposure and erosion testing are being manufactured and delivered to work package 4 (CIEMAT, CVR, Julich). These tests are relevant to the CSP heat exchanger environment and include erosion using ceramic particles, long-term oxidation, CO_2 and s-CO_2 exposures.